Efficiency improvement of phosphorescent organic light-emitting diodes using semitransparent Ag as anode

H. J. Peng, X. L. Zhu, J. X. Sun, X. M. Yu, M. Wong, and H. S. Kwok[a)]
Center for Display Research, Department of Electrical and Electronic Engineering, Hong Kong University of Science and Technology, Clear Water Bay, Hong Kong

(Received 22 July 2005; accepted 15 November 2005; published online 19 January 2006)

The emission efficiency in an organic light-emitting diode (OLED) based on fac tris(phenyl pyridine)iridium [$Ir(ppy)_3$] is greatly improved using a semitransparent Ag anode. With surface modification of the Ag anode, excellent light coupling and hole injection properties can be realized. The Ag-based OLED exhibits a maximum current efficiency of 81 cd/A and a power efficiency of 79 lm/W, compared with 46 cd/A and 39 lm/W for an indium-tin oxide anode device, respectively. © *2006 American Institute of Physics*. [DOI: 10.1063/1.2164901]

Through harvesting both singlet and triplet excitons, the internal emission quantum efficiency of organic light-emitting diodes (OLEDs) doped with phosphorescent emitters can reach nearly 100%.[1,2] However, the problem remains that a large fraction of the generated light is trapped by total internal reflection and is never emitted from the device. The typical light coupling efficiency of an OLED is only ~20%.

There are several methods reported in the literature to improve the coupling efficiency of OLEDs, such as using microcavity, microlens array, low index substrate, nanopatterned photonic crystals, etc.[3–7] They all have their merits and drawbacks. The microcavity structure has been studied the most because it does not involve too much extra effort in fabricating the device. A microcavity OLED typically uses a distributed Bragg reflector (DBR).[3,4] However, the multilayer dielectric thin-film structure of the DBR makes the fabrication process complicated. As well, the thickness of the DBR makes the angular color shift intolerably large. The alternative design of utilizing a single semitransparent metal layer as the reflector is more desirable.

Semitransparent metal reflectors with low absorption have been used in top-emitting OLEDs as the top cathode. These top-emitting devices also demonstrated higher coupling efficiency than an equivalent bottom-emitting nonmicrocavity device due to a strong microcavity effect.[8–11] Here we use a semitransparent metal as the anode in a bottom emitting device.

There are two issues with using a metallic anode: (1) The hole injection efficiency has to be improved, and (2) the microcavity has to be optimized. In this letter, we demonstrate a bottom-emitting microcavity OLED employing a semitransparent Ag film as the anode and opaque Al as the cathode. Using a phosphorescent material, $Ir(ppy)_3$, the Ag anode devices exhibit a maximum efficiency of 81±8 cd/A and a power efficiency of 79±8 lm/W. This is much better than the results of 46±4.5 cd/A and 39±4 lm/W for a similar ITO anode device.

The ITO and Ag OLEDs are first optimized by a model calculation of the power emitted into different optical modes. The device structure is shown in Fig. 1(a). The optics of a planar OLED are analyzed by a classical model based on the equivalence between the emission of a photon due to exciton radiative decay and the radiation of a classical electrical dipole.[12–14] In this model, the power generated, $\bar{P}$ by a dipole source can be expressed as an integral over the in-plane wave vector $k_{\|}$,

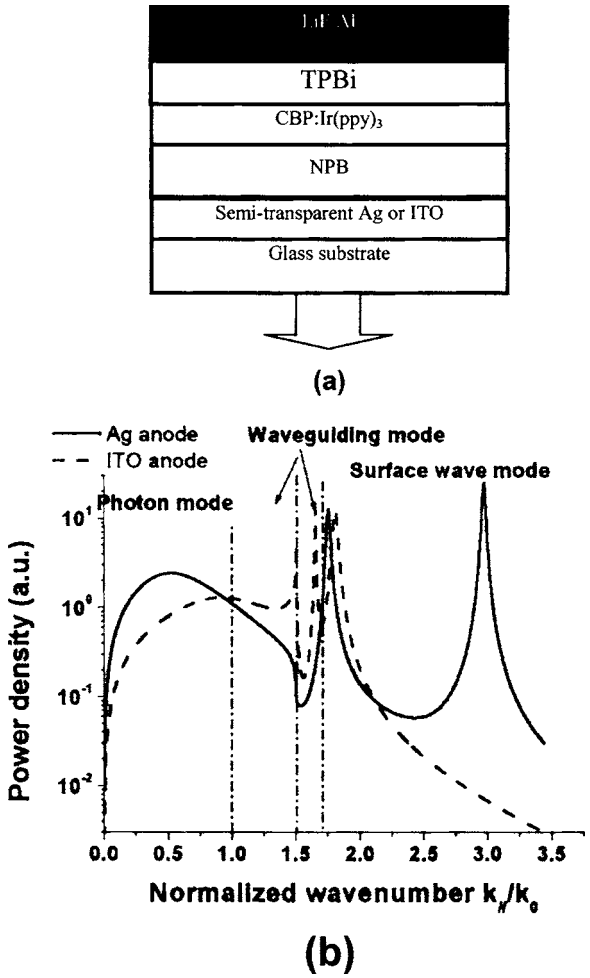

FIG. 1. (a) Structures of bottom-emitting phosphorescent OLEDs using Ag or ITO as anode. (b) The $k_{\|}$-space spectra at a dipole embedded in ITO anode device with a structure of ITO (75 nm)/NPB(70 nm)/CBP: $Ir(ppy)_3$(8 wt %,25 nm)/TPBi(40 nm)/LiF(1 nm)/Al(110 nm) and Ag anode device with structure of Ag (25nm)/NPB(52 nm)/CBP: $Ir(ppy)_3$(8 wt %,20nm)/TPBi(40 nm)/LiF(1 nm)/Al(110 nm).

[a)]Electronic mail: eekwok@ust.hk

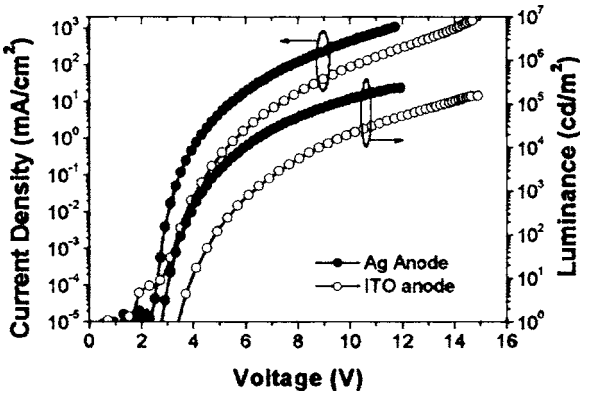

FIG. 2. *J-V-L* characteristics of Ag anode and ITO anode phosphorescent OLEDs.

$$\bar{P} = \int_0^\infty K(k_\parallel) dk_\parallel, \tag{1}$$

where the quantity $K(k_\parallel)$ is defined as the $k_\parallel$-space power spectrum. The distribution of the radiation power into different plane wave modes can be identified with different regions of this $k_\parallel$ integration. The calculated power can be used as a benchmark for optimizing device layer thicknesses to improve coupling efficiency. In addition, comparing the fraction of the light in each mode type lends insight into how the Ag anode device can improve the coupling efficiency.

Figure 1(b) shows the calculated $k_\parallel$-space power spectra for the cases of an ITO anode device and an Ag anode device, where the dipole is located at the emission zone with random orientation. The power spectra can be divided into four regions according to the $k_\parallel$ value. Region I ($0 \leqslant k_\parallel \leqslant k_0$),[15] corresponds to the photon emission mode, i.e., it gives the portion of the total light that can be extracted from the device surface as useful radiation. Regions II ($k_0 \leqslant k_\parallel \leqslant 1.5k_0$) and III ($1.5k_0 \leqslant k_\parallel \leqslant 1.7k_0$) correspond to waveguiding loss in the glass substrate and the organic/ITO layers, respectively. Narrow peaks in Region IV ($1.7k_0 \leqslant k_\parallel$) are the surface wave modes, corresponding to evanescent surface waves propagating along the metallic electrode surface.[14] It can be seen that for the Ag anode structure, the power density of the photon mode is much higher than that of the conventional ITO anode structure. At the same time, the power densities of waveguide modes in both glass and organic layers are significantly suppressed. Comparing the integrated power in the photon modes of the two devices, we expect an enhancement factor of 1.7 from the Ag anode device.

Two bottom-emitting OLEDs with different anodes were fabricated to verify the theoretical predictions. The ITO anode device was deposited on an ITO-coated glass substrate having an ITO thickness of 750 Å and a sheet resistance of 25 Ω/sq. The ITO surface was modified by the usual oxygen plasma to enhance its hole injection ability. For the Ag anode device, a 250 Å thick Ag film was deposited on a glass substrate by thermal evaporation with a sheet resistance of 1.6 Ω/sq.

One challenge to using Ag as the anode is its relatively low work function of 4.3 eV,[16] which leads to a large barrier for hole injection into the organic layer. In order to enhance the hole injection ability, the Ag anode surface was modified using a CF_4 plasma. An ultrathin CF_x layer was formed on the Ag surface after the CF_4 plasma pretreatment, effectively reducing the carrier injection barrier. This CF_x layer has been studied using x-ray photoemission spectroscopy (XPS) in Ref. 17. Interestingly, it was found that the CF_4 plasma pretreatment was effective regardless of whether or not the Ag surface had been exposed to air. Thus this CF_x layer is quite robust and can be useful in the manufacturing process.

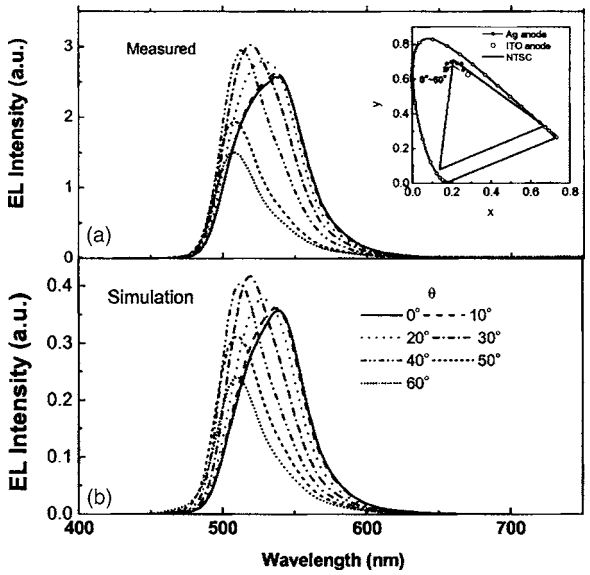

FIG. 3. (a) The measured and (b) simulated EL spectra of the Ag anode device for viewing angles from 0° to 60°. Inset of (a), 1931 CIE coordinates of the spectra.

In both devices, we used 4,4′-bis(1-napthyl-*N*-phenyl-amino)-biphenyl (NPB) as the hole transport layer, 4,4′-*N*,*N*′-dicarbazole-biphenyl (CBP) doped with fac tris (2-phenylpyridine) iridium [$Ir(ppy)_3$] as the emitter layer, 1,3,5-tris (*N*-phenylbenzimidazol-2-yl)benzene (TPBi) as the electron injection layer, and LiF/Al as the composite cathode. The ITO anode device consists of ITO (75 nm)/NPB(70 nm)/CBP:$Ir(ppy)_3$(8 wt %,25 nm)/TPBi(40 nm)/LiF(1 nm)/Al(110 nm). The Ag anode device consists of Ag (25 nm)/NPB(52 nm)/CBP:$Ir(ppy)_3$(8 wt %,20 nm)/TPBi (40 nm)/LiF(1 nm)/Al(110 nm). The layer thicknesses of both devices have been optimized based on the microcavity model. For the Ag anode device, both anode and organic layer thicknesses were carefully tuned to balance the coupling efficiency enhancement and emission color variation. All layers, including the semitransparent Ag, were deposited by thermal evaporation in a multichamber vacuum system without breaking the vacuum.

The current density (*J*)-voltage (*V*)-luminance (*L*) characteristics of both devices were measured using an HP4145B semiconductor parameter analyzer and a large diameter (2.5 cm) photodiode. The external quantum efficiencies of the devices were measured directly by placing the device about 2 mm over the photodiode. The spectral characterization and the luminance calibration of the photodiode were carefully performed with a PhotoResearch PR650 spectroradiometer. In the measurement, a Lambertian distribution is assumed for the ITO anode device while the non-Lambertian emission profile has been taken into account for the Ag anode device.

Figure 2 compares the *J-V-L* of the devices with the voltage drop in the electrodes was subtracted out. The volt-

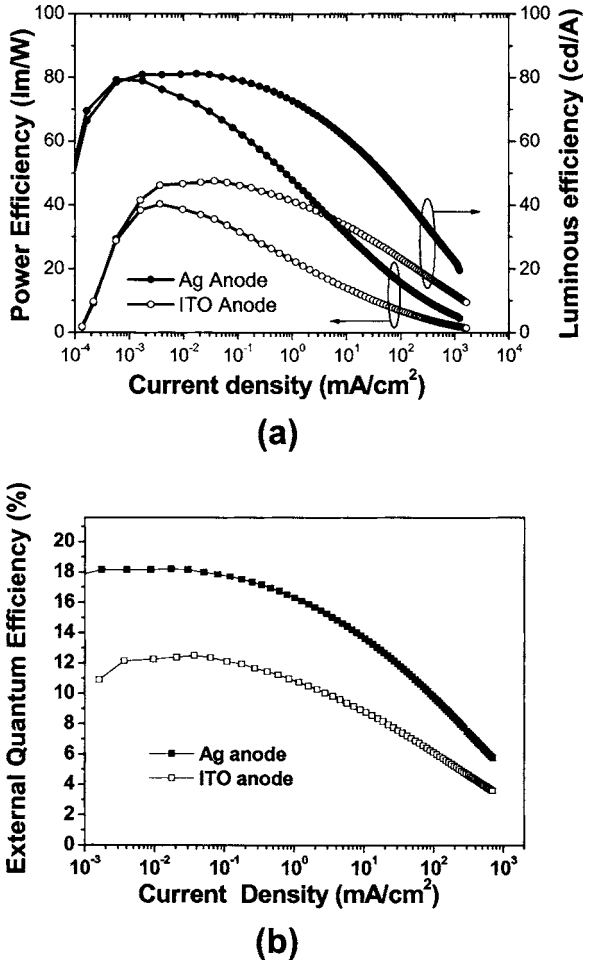

FIG. 4. (a) Power efficiency (η_P) and the current efficiency (η_J) of the Ag anode and ITO anode devices, and (b) comparison of the external quantum efficiency of both devices.

age drop along the electrodes was calculated by multiplying the injection current and the electrode resistances, which were 5 Ω and 80 Ω for the Ag anode and ITO anode devices, respectively. It can be seen that the Ag anode device shows a performance superior to that of the ITO anode device in both the *L-V* and *J-V* curves.

Figure 3(a) shows the EL spectra measured under a current of 2 mA/cm^2 at viewing angles from 0° to 60° for the Ag anode device. When the viewing angle increases, the emission peak shifts from 536 nm to 512 nm. Although there is some spectral shift, the corresponding 1931 CIE color coordinates are still quite close to the NTSC standard green, as shown in the inset of Fig. 3(a). The simulated electroluminescence (EL) spectra are given in Fig. 3(b). It can be seen that the measured spectrum and relative intensities agree quite well with the calculated ones, confirming the accuracy of the simulation.

Figure 4(a) shows the power efficiency (η_P) and the current efficiency (η_J) of both devices. The maximum η_J and η_P of the Ag anode device are 81±8 cd/A and 79±8 lm/W, respectively; and are 46±5 cd/A and 39±4 lm/W for the ITO anode device. At the luminance of 1000 cd/m^2, the Ag anode device still demonstrates a high power efficiency of 47±5 lm/W, compared with that of 21±2 lm/W for the ITO anode device.

The superior performance of the Ag anode device can be attributed to the enhanced hole injection and more efficiency outcoupling of light in the microcavity structure. Figure 4(b) shows the current density dependence of the external quantum efficiency η_{EQE} for both devices. An efficiency of 12.3% at 10 μA/cm^2 was achieved from the ITO anode device, similar to the recently reported results by Liao *et al.*[18] Under the same current density, the efficiency was 18.1% for the Ag anode device, indicating a 45% enhancement of the coupling efficiency assuming the same charge balance factors in both devices. Although this increase is slightly less than the modeling result, it is encouraging and lends support to the model.

In conclusion, we have demonstrated a high efficiency electrophorphorescent OLED using semitransparent Ag as the anode. The microcavity structure formed by the semitransparent anode and a reflective cathode can effectively enhance the coupling efficiency of the device. The experimental results indicate an increase of 45±5%. Moreover, with proper surface modification, the hole injection ability of the anode can be enhanced significantly as well. The results show that the maximum η_J and η_P of the Ag anode device are 81±8 cd/A and 79±8 lm/W, respectively. We believe that a power efficiency over 100 lm/W can be achieved by combining this microcavity structure and more efficient phosphorescent emitting materials.[1,2]

This work was supported by the Hong Kong Government Innovations and Technology Commission.

[1]C. Adachi, M. A. Baldo, M. E. Thompson, and S. R. Forrest, J. Appl. Phys. **90**, 5048 (2001).
[2]M. Ikai, S. Tokito, Y. Sakamoto, T. Suzuki, and Y. Taga, Appl. Phys. Lett. **79**, 156 (2001).
[3]R. H. Jordan, L. J. Rothberg, A. Dodabalapur, and R. E. Slusher, Appl. Phys. Lett. **69**, 1997 (1996).
[4]H. J. Peng, M. Wong, and H. S. Kwok, SID Int. Symp. Digest Tech. Papers **34**, 516 (2003).
[5]S. Möller and S. R. Forrest, J. Appl. Phys. **91**, 3324 (2002).
[6]T. Tsutsui, M. Yahiro, H. Yokogawa, K. Kawano, and M. Yokoyama, Adv. Mater. (Weinheim, Ger.) **13**, 1149 (2001).
[7]C. W. Chen, P. Y. Hsieh, H. H. Chiang, C. L. Lin, H. M. Wu, and C. C. Wu, Appl. Phys. Lett. **83**, 5127 (2003).
[8]Y. J. Lee, S. H. Kim, J. Huh, G. H. Kim, Y. H. Lee, S. H. Cho, Y. C. Kim, and Y. R. Do, Appl. Phys. Lett. **82**, 3779 (2003).
[9]M. H. Lu and J. C. Sturm, J. Appl. Phys. **92**, 595 (2002).
[10]C. Qiu, H. J. Peng, Z. L. Xie, H. Y. Chen, M. Wong, and H. S. Kwok, SID Int. Symp. Digest Tech. Papers **35**, 974 (2003).
[11]H. Riel, S. Karg, T. Beierlein, B. Ruhstaller, and W. Rieß, Appl. Phys. Lett. **82**, 466 (2003).
[12]W. Lukosz, Phys. Rev. B **22**, 3030 (1980).
[13]K. Neyts, P. de Visschere, D. K. Fork, and G. B. Anderson, J. Opt. Soc. Am. B **17**, 114 (2000).
[14]G. W. Ford and W. H. Weber, Phys. Rep. **113**, 195 (1984).
[15]The wave number k_0 is determined by $k_0=2\pi/\lambda_0$, λ_0 is set to be 520 nm, a little larger than the peak wavelength of photoluminescence spectrum of emitting material which is 512 nm for Ir(ppy)$_3$.
[16]H. B. Michaelson, IBM J. Res. Dev. **22**, 72 (1978).
[17]H. J. Peng, X. L. Zhu, J. X. Sun, X. M. Yu, M. Wong, and H. S. Kwok, Appl. Phys. Lett. **87**, 173505 (2005).
[18]L. S. Liao, K. P. Klubek, and C. W. Tang, Appl. Phys. Lett. **84**, 167 (2004).